

*to appear in The Astronomical Journal (March 1999)*

## **New High-Redshift Radio Galaxies from the MIT-Green Bank Catalog<sup>1</sup>**

Daniel Stern

Astronomy Department, University of California at Berkeley, CA 94720

Electronic Mail: dan@copacabana.berkeley.edu

Arjun Dey<sup>2</sup>

Dept. of Physics and Astronomy, The Johns Hopkins University, 3400 N. Charles St., Baltimore,  
MD 21218

Electronic Mail: dey@skysrv.pha.jhu.edu

Hyron Spinrad & Leslie Maxfield

Astronomy Department, University of California at Berkeley, CA 94720

Electronic Mail: spinrad@bigz.berkeley.edu, lmm@astron.berkeley.edu

Mark Dickinson<sup>3</sup>

Dept. of Physics and Astronomy, The Johns Hopkins University, 3400 N. Charles St., Baltimore,  
MD 21218

Electronic Mail: med@stsci.edu

David Schlegel

Department of Astrophysical Sciences, Princeton University, Princeton, NJ 08544

Electronic Mail: schlegel@astro.princeton.edu

Rosa A. González

Space Telescope Science Institute, Baltimore, MD 21218

Electronic Mail: ragl@stsci.edu

---

<sup>1</sup>Based on observations obtained at the W.M. Keck Observatory, Lick Observatory, and the MDM Observatory. The Keck Observatory is operated as a scientific partnership among the University of California, the California Institute of Technology, and the National Aeronautics and Space Administration, and was made possible by the generous financial support of the W.M. Keck Foundation.

<sup>2</sup>Hubble Fellow.

<sup>3</sup>Alan C. Davis Fellow, also at the Space Telescope Science Institute.

## ABSTRACT

We present optical identifications and redshifts for seventeen new high-redshift radio sources. Fifteen of these sources are radio galaxies; the remaining two are high-redshift, steep-spectrum, radio-loud quasars. These objects were discovered as part of an ongoing study of compact ( $\theta < 10''$ ), moderately steep spectrum ( $\alpha_{1.4 \text{ GHz}}^{4.8 \text{ GHz}} > 0.75, S_\nu \propto \nu^{-\alpha}$ ) sources from the MIT – Green Bank (MG) radio catalog ( $S_{5 \text{ GHz}} \gtrsim 50 \text{ mJy}$ ). Spectra for the optical counterparts were obtained at the W.M. Keck Telescopes and are among the optically faintest radio galaxies thus far identified. Redshifts range between 0.3 and 3.6, with thirteen of the seventeen at redshifts greater than 1.5. Combining these new radio galaxies with two published MG radio galaxy spectra, we synthesize a composite MG radio galaxy spectrum and discuss the properties of these galaxies in comparison to other, more powerful, radio galaxies at similar redshifts. We suggest a radio power—ionization state relation.

*Subject headings:* cosmology: early universe — galaxies: active — galaxies: redshifts — galaxies: evolution – radio continuum: galaxies

## 1. Introduction

The MIT – Green Bank (MG) survey (Bennett et al. 1986; Lawrence et al. 1986) consists of 5974 radio sources in 1.87 steradians of sky in an equatorial strip which have flux densities  $\gtrsim 50$  mJy at 5 GHz. Studies of higher-flux density radio surveys such as the 3CR (Spinrad & Djorgovski 1987), Molonglo (McCarthy et al. 1996), and B2/1 Jy of Allington-Smith (1982) have yielded many interesting discoveries, such as the radio-optical alignment of high-redshift radio galaxies (Chambers et al. 1987; McCarthy et al. 1987), very high-redshift galaxies (e.g., Lacy et al. 1995; Spinrad, Dey, & Graham 1995; Rawlings et al. 1996), and rich clusters at high-redshift (e.g., Dickinson 1996). The MG survey probes the parameter space between high flux density surveys such as the 3CR, and milli- and micro-Jansky surveys such as the Leiden Berkeley Deep Survey and its extensions (Neuschaefer & Windhorst 1995). The MG range of radio flux density is also considered by the B3 survey (Vigotti et al. 1989) and recent Cambridge surveys (e.g., 6C — Hales, Baldwin, & Warner 1993), but the MG survey was conducted at a higher frequency than these other surveys. Selecting an intermediate power sample allows us to study various properties as a function of radio power. In particular, a lower radio power suggests these galaxies may, on average, be less dominated by their active nuclei, and may thus be more representative of giant ellipticals at large redshift (cf., Dunlop et al. 1996; Spinrad et al. 1997; Dey et al. 1998). Fainter flux densities also suggest that a fraction of our sample may be at very high redshift, and indeed the median redshift of radio galaxies in the MG observed to this point is  $z_{\text{med}} \sim 1.1$  compared to  $z_{\text{med}} = 0.27$  for the 3CR (McCarthy 1993).

Over the past several years we have been pursuing the optical identification of a subset of 218 radio sources systematically selected from the MG catalog. We restrict our sample to radio sources of small angular size ( $\theta \leq 10''$ ), simple (unresolved, double, or triple) radio morphology, and moderately steep radio spectral index ( $\alpha_{1.4}^{4.8 \text{ GHz}} > 0.75$ ,  $S_\nu \propto \nu^{-\alpha}$ ). The size and morphological criteria primarily select against objects at low redshift. The angular size limit should also bias the sample to larger lookback times when the higher density of the intergalactic medium is more effective at confining radio lobes. The spectral index criterion eliminates low-redshift interlopers and selects against flat-spectrum quasars and in favor of radio galaxies, but is only moderately restrictive amongst the radio galaxies themselves (Blumenthal & Miley 1979). Resulting identifications are often very distant objects and thus serve as useful probes for the study of galaxy formation and evolution. In combination with other complete samples, such as the 3CR, optical and near-IR properties of MG sources can be used in correlative studies which span a range of radio power at any given redshift. Similar studies suggest that weak radio sources ( $S_{1.4\text{GHz}} < 50$  mJy) have weaker emission lines and the alignment effect becomes less pronounced with lower radio flux density samples (e.g., Rawlings & Saunders 1991; Dunlop & Peacock 1993; Eales & Rawlings 1993; Thompson et al. 1994). McCarthy (1993) has recently presented a comprehensive review on the optical and associated properties of radio galaxies.

Preliminary results from our survey are described in Spinrad et al. (1993), Dey, Spinrad, & Dickinson (1995), and Stern et al. (1996; 1997). Currently, we have optical identifications for

$\sim 85\%$  of our sample and spectroscopic redshifts for  $\gtrsim 60\%$  of the sample. In this paper we report on seventeen new identifications and redshifts of MG sources. The spectra were obtained at the W.M. Keck Telescopes and are representative of some of the fainter radio identifications thus far. Typical  $R$  magnitudes are 23 – 24. Many of these sources are in the so-called ‘redshift desert,’  $1.4 \lesssim z \lesssim 2.0$ , for which no strong features (i.e., Ly $\alpha$ , [O II]  $\lambda 3727$ , or H $\alpha$ ) are redshifted into the optical window, thus making redshift determinations challenging. Our MG sample currently includes 13 galaxies with  $z > 2$ ; we report on 4 such galaxies here.

The paper is organized as follows: in §2 we present the observations and data reductions, followed by a discussion of individual systems in §3. We construct a composite spectrum and compare it with models and other composite spectra of active galaxies in §4. A concluding discussion comprises §5. Throughout this paper we adopt  $H_0 = 50 h_{50} \text{ km s}^{-1} \text{ Mpc}^{-1}$ ,  $q_0 = 0.5$ , and  $\Lambda = 0$  unless otherwise noted.

## 2. Observations and Data Reduction

### 2.1. Imaging and Optical Identifications

Preliminary imaging observations of all sources were made over the course of several years (1988 – 1998) at the Lick Observatory 3m Shane Telescope on Mount Hamilton and the MDM 2.4m Hiltner Telescope at Kitt Peak. The Kast Double Spectrograph of Lick Observatory (Miller & Stone 1994) employs UV-flooded Reticon 1200x400 CCDs with  $27\mu\text{m}$  pixels, corresponding to a plate scale of  $0''.78 \text{ pix}^{-1}$ . Typical seeing for the Lick imaging was  $1''.2 - 1''.8$ . The Charlotte camera of MDM employs a Tek 1024<sup>2</sup> CCD detector with a plate scale of  $0''.275 \text{ pix}^{-1}$ . Typical seeing for these images was  $1''.0 - 1''.5$ .

A subsample of seven of the seventeen sources were later reimaged with the Low Resolution Imaging Spectrometer (LRIS; Oke et al. 1995) at the 10m W.M. Keck Telescopes on Mauna Kea between 1994 and 1998. The detector is a Tek 2048<sup>2</sup> CCD with  $24\mu\text{m}$  pixels. Due to a dewar change in July 1996, the pixel scale changed from  $0''.214 \text{ pix}^{-1}$  to  $0''.212 \text{ pix}^{-1}$  at that time. The typical seeing was  $0''.8 - 1''.0$ . A journal of our observations is provided in Table 1.

The images were corrected for overscan bias, flattened using a median sky flat, coadded, and calibrated using observations of standard stars. Utilizing astrometry provided by B. Burke and S. Conner, we obtained optical identifications for our candidates based upon the radio coordinates. Typically the optical morphologies are small, faint, and round. We present finding charts in Fig. 1 (Plates 1 – 3). Where available, we present Keck images; the remaining images were obtained at Lick and the MDM as indicated in Table 1. Astrometry for each identification is tabulated in Table 2 with the coordinates of the offset star provided. The estimated uncertainty in the optical positions is  $0''.3$ . Optical and radio properties of the sources are in Table 3, where the radio flux densities and spectral indices are from Bennett et al. (1986) and Lawrence et al. (1986). Radio luminosities

have been calculated at a rest-frame frequency of 4.8 GHz, implementing the spectral index derived from 1.4 and 4.8 GHz observations, a Hubble constant of  $H_0 = 50 h_{50} \text{ km s}^{-1} \text{ Mpc}^{-1}$ ,  $q_0 = 0$ , and  $\Lambda = 0$ . In Table 4 we include more recent 4.85 GHz flux densities for the sample. Many sources may vary at the 10% level over the 10 year baseline, though MG 2058+0542 apparently varied considerably more over the same period. We therefore indicate its spectral index as uncertain in Table 3. Magnitudes, measured in site-dependent apertures as described in Table 3, are from our CCD photometry and have errors of  $\sim 0.1$  to  $0.3$  magnitudes. Observations obtained at Lick Observatory employed the Spinrad night-sky filter and yield red magnitudes in the  $R_S$  system, which is related to commonly used photometric systems by Djorgovski (1985)<sup>1</sup>. Typical optical magnitudes are  $R \sim 23 - 24$ , probing the fainter envelope of our MG survey.

## 2.2. LRIS Spectroscopy

We obtained spectroscopic observations with LRIS between 1994 and 1997. We generally used a 300  $\ell/\text{mm}$  grating (blazed at 5000 Å) to sample a wavelength range  $\lambda\lambda 4000-9000$  Å, and a 1 arc-second wide slit which yields an effective resolution FWHM of  $\approx 10$  Å. The read noise and gain were typically  $8.0e^-$  and  $1.6e^- \text{ adu}^{-1}$  respectively. However, during the 1994 March run, the LRIS CCD was affected by pattern noise which mimicked extremely high read noise ( $25e^-$  and  $65e^-$  on the blue and red sides), noticeably degrading the spectrum of MG 1251+1104. Observations were typically done at an airmass  $\lesssim 1.05$ . Hence, although the slit position angle was often selected to trace the radio morphology or to include nearby optical sources, we believe our relative spectrophotometry to be accurate for the wavelengths considered (cf., Filippenko 1982). The sources attempted spectroscopically at Keck were primarily selected from the fainter ( $R \gtrsim 23$ ) identifications in the MG survey, many having been unsuccessful spectroscopic targets at Lick Observatory. Exceptions are the relatively bright sources MG 0422+0816 ( $R \sim 20$ ) and MG 0511+0143 ( $R \sim 22$ ) which were first observed spectroscopically as a backup project at Keck Observatory on an inclement night. These observations utilized a 600  $\ell/\text{mm}$  grating (blazed at 5000 Å). The bright quasar MG 2041+1854 ( $R \sim 20$ ) was observed at Keck during twilight on a cirrusy night, while the relatively bright ( $R_S \sim 21$ ) sources MG 0148+1028 and MG 0308+0720 were first surveyed spectroscopically as backup targets on 23 December 1997 UT.

For each observation, we offset the telescope from the reference star listed in Table 2. The data were corrected for overscan bias, flat-fielded using internal lamps taken after each observation, flux calibrated using observations of spectrophotometric standard stars (Massey et al. 1988; Massey & Gronwall 1990), and corrected for Galactic reddening using the Burstein & Heiles (1982) maps (see Table 3) with the Cardelli, Clayton, & Mathis (1989) extinction curve. One-dimensional spectra were extracted with a typical aperture size of  $1''.4$ . The standard stars were observed both with and

---

<sup>1</sup>The transformation from Spinrad night-sky  $R_S$  into Johnson  $VR$  is  $(R_S - R) = -0.004 - 0.072(V - R) + 0.073(V - R)^2$ .

without an OG570 filter in order to correct for the second order light contaminating the wavelength region  $\lambda > 7500 \text{ \AA}$ . A journal of the observations is provided in Table 1 and individual spectra are presented in Fig. 2 with the prominent features indicated. In Table 5 we list the line flux densities measured for each source. For completeness, we include the only two published spectra of MG radio galaxies (MG 1019+0534 — Dey, Spinrad, & Dickinson 1995; MG 2144+1928 — Maxfield et al. 1998) in Fig. 2 and Table 5.

### 3. Notes on Individual Sources

*MG 0018+0940*, at  $z=1.586$ , exhibits a low ionization spectrum: unlike more powerful radio sources, the C III]  $\lambda 1909$  line is stronger than the C IV  $\lambda\lambda 1549$  doublet. Mg II  $\lambda\lambda 2800$  is clearly resolved. The optical ( $R$ ) image of MG 0018+0940 has an extended, chain-like morphology oriented at a position angle of  $137^\circ$  in the optical. The radio source is unresolved in 4.85 GHz observations with the B-array of the VLA ( $\sim 1''.2$  beam; Lawrence et al. 1986).

*MG 0046+1102*, at  $z=1.813$ , also exhibits a low ionization spectrum, with similar carbon and magnesium line strengths to MG 0018+0940. Mg II  $\lambda\lambda 2800$  is again a strong and clearly resolved feature. The optical identification is extended with a position angle of  $130^\circ$  in  $R$ , while the source is unresolved in 4.85 GHz observations obtained with the B-array configuration of the VLA.

*MG 0122+1923*, at  $z=1.595$ , also exhibits a low ionization spectrum, with carbon line strengths similar to the prior two radio galaxies. The optical identification contains a compact core and diffuse emission to the North oriented at a position angle of  $41^\circ$ .

*MG 0148+1028*, at  $z=2.845$ , is an intriguing source showing both the bright emission lines typical of high-redshift radio galaxies and the narrow absorption lines that characterize high-redshift, star-forming galaxies (cf., Steidel et al. 1996, Lowenthal et al. 1997). These lines, indicated with vertical dashed lines in Fig. 2, refer to Si II  $\lambda 1260$ , O I  $\lambda 1302$ , C II  $\lambda 1335$ , Si IV  $\lambda\lambda 1394, 1403$ , S V  $\lambda 1502$ , Si II  $\lambda 1526$ , Fe II  $\lambda 1608$ , and Al II  $\lambda 1670$  (e.g., Spinrad et al. 1998). The emission lines of this source are slightly broader than in those sources considered above, with FWHM  $\sim 1000 \text{ km s}^{-1}$  — a value commonly seen in quasars, though the low C IV  $\lambda\lambda 1549$ /He II  $\lambda 1640$  ratio leads us to classify this source as a broad-lined radio galaxy. A detailed analysis of MG 0148+1028 is deferred to future publication; note, however, that S V  $\lambda 1502$ , an unambiguous signature of starlight (e.g., Dey et al. 1997), is visible in absorption. The finding chart for this galaxy derives from a short (60s) exposure obtained through LRIS without a filter to identify the field; this image is superior to the 1260s Lick image. Slit spectroscopy was done at a position angle of  $138^\circ$  so that galaxies b and c (see Fig. 1) would also be observed. Neither is associated with MG 0148+1028; galaxy b has [O II]  $\lambda 3727$  and [O III]  $\lambda\lambda 4959, 5007$  in emission at  $z = 0.588$ , while galaxy c has [O II]  $\lambda 3727$  in emission with Mg II  $\lambda\lambda 2800$  in absorption at  $z = 1.297$ . The optical identification is marginally resolved:  $\text{FWHM}_{\text{MG}} \approx 1''.0$ , while the seeing was  $\approx 0''.9$ .

*MG 0308+0720*, at  $z=2.975$ , is a radio-loud quasar as evidenced by the broad emission lines

(e.g.,  $\text{FWHM}(\text{C IV}) \sim 5600 \text{ km s}^{-1}$ ) and unresolved morphology. The  $\text{Ly}\alpha$ – $\text{N V } \lambda 1240$  emission complex is unusual, with narrow  $\text{Ly}\alpha$  superimposed upon a broad  $\text{N V } \lambda 1240$  emission line. Recent statistical investigations of broad UV lines in luminous (radio–quiet) quasars have suggested that the traditional broad–line region (BLR) consists of two components — a low–density, intermediate–line region (ILR;  $\text{FWHM} \sim 2000 \text{ km s}^{-1}$ ) and a higher density, very broad line region (VBLR;  $\text{FWHM} \gtrsim 7000 \text{ km s}^{-1}$ ) blueshifted by  $\gtrsim 1000 \text{ km s}^{-1}$  with respect to the ILR (e.g., Brotherton et al. 1994). Differences in the relative contributions of these two components can explain much of the observed variation in quasar broad–line profiles. For instance,  $\text{Ly}\alpha$  will come predominantly from the ILR, while higher ionization lines such as  $\text{N V } \lambda 1240$ ,  $\text{Si IV } \lambda\lambda 1394, 1403$ , and  $\text{C IV } \lambda\lambda 1549$  are dominated by VBLR emission. In this simple model, MG 0308+0720 is a quasar whose broad–lines are dominated by the VBLR; indeed, the  $\text{Ly}\alpha$  spectral profile looks similar to that of the composite VBLR presented in Fig. 2a of Brotherton et al. (1994). Alternatively, we may be seeing a dusty quasar at high redshift. The  $\text{Ly}\alpha$ – $\text{N V } \lambda 1240$  complex is dominated by broad  $\text{N V } \lambda 1240$  emission. Subtracting a Gaussian fit to the  $\text{N V } \lambda 1240$  line, we find the residual  $\text{Ly}\alpha$  to be extremely weak: the  $\text{Ly}\alpha/\text{C IV } \lambda\lambda 1549$  ratio is  $\sim 0.25$ , compared to a mean value of  $1.2 - 2.2$  in composite quasar spectra (Boyle 1990; Francis et al. 1991). The extremely red continuum is in concordance with this dust–obscuration interpretation. Three  $\text{Mg II } \lambda\lambda 2800$  absorption systems at redshifts  $z = 1.391, 1.607$ , and  $1.814$  are also evident in the spectrum.

*MG 0311+1532*, at  $z=1.989$ , exhibits a slightly higher ionization spectrum in comparison to the above radio galaxies.  $\text{C II] } \lambda 2326$  is barely apparent as a faint broad bump near  $7000 \text{ \AA}$ . The red continuum of this source, and particularly the abrupt feature at  $7150 \text{ \AA}$  are likely artifacts due to scattered light from a bright star  $3''.5$  to the NE. The optical identification consists of low surface brightness emission oriented at a position angle of  $135^\circ$ , while the  $4.8 \text{ GHz}$  morphology is extended by  $5''.1$  at a position angle of  $161^\circ$ .

*MG 0422+0816*, at  $z=0.289$ , was observed spectroscopically at Keck as a backup object on a night of poor seeing and thick cirrus, thus making our primary faint targets untenable. The relatively bright optical flux ( $R \sim 20$ ) and unfluxed spectrum are the byproducts of these meteorological conditions which prevented observations of our primary fainter targets. The  $[\text{O III}] \lambda\lambda 4959, 5007$  nebular lines are the most prominent feature of the spectrum. The optical counterpart consists of a marginally resolved core with diffuse emission to the south.

*MG 0511+0143*, at  $z=0.596$ , was also observed as a back–up target on an inclement night. This galaxy has a weak–lined spectrum with  $[\text{O II}] \lambda 3727$  of low equivalent width and a prominent  $4000 \text{ \AA}$  break (labeled with an arrow in Fig. 2), indicative of an old stellar population. MG 0511+0143 was also imaged in the J and K' bands at Lick Observatory on cirrusy nights. Comparing the multiband images suggests the radio galaxy may be part of a cluster at  $z \sim 0.6$ . The vignetting of the finding chart is due to the small field–of–view of the Kast imaging spectrometer on the Lick 3m. The optical identification is oriented at a position angle of  $48^\circ$ , while the  $4.8 \text{ GHz}$  morphology is extended by  $3''.9$  at a position angle of  $171^\circ$ .

*MG 1019+0534*, at  $z=2.765$ , has an unusual spectrum which is previously reported in Dey, Spinrad, & Dickinson (1995).  $\text{Ly}\alpha$ , usually the strongest line in high-redshift radio galaxies, is very weak. This is likely due to dust attenuating the  $\text{Ly}\alpha$  emission, implying dust formation at early epochs for this system.

*MG 1142+1338*, at  $z=1.279$ , is a weak-lined radio galaxy with strong  $[\text{O II}] \lambda 3727$  and high ionization  $[\text{Ne V}] \lambda 3426$ .  $\text{C III}] \lambda 1909$  is barely visible as a broad feature while neither  $\text{C II}] \lambda 2326$  nor  $\text{Mg II } \lambda \lambda 2800$  are visible. The optical counterpart is compact.

*MG 1251+1104*, at  $z=2.322$ , was observed during the 1994 March run when the LRIS CCD was compromised by high pattern noise.  $\text{Ly}\alpha$  is the dominant feature of the spectrum. The continuum slope is untrustworthy and a relic of instrumental problems, and lead to uncertain equivalent widths in Table 5. The optical morphology is diffuse and symmetric.

*MG 1401+0921*, at  $z=2.093$ , exhibits a moderate ionization spectrum radio galaxy with strong  $\text{C III}] \lambda 1909$  and weak  $\text{C II}] \lambda 2326$ . The optical counterpart is slightly elongated with a shell structure to the NW, while the radio morphology has a classic double structure of separation  $3''.5$  at a position angle of  $138^\circ$ . A similar asymmetric optical structure is observed in  $V$ -band images of 4C 23.56 (Knopp & Chambers 1997). Deep multi-band images lead them to interpret the morphology of 4C 23.56 as deriving from a dusty galaxy illuminated by a beam from an active nucleus which is scattered into our line of sight.

*MG 2037–0011*, at  $z=1.512$ , is a weak-lined source showing several faint emission lines. Most strikingly, the  $\text{C III}] \lambda 1909$  line has a narrow component superimposed upon a broad component. A comparison with the similar redshift radio galaxy MG 0018+0940 is interesting — in particular, note that  $\text{Mg II } \lambda \lambda 2800$  is not seen in the spectrum of MG 2037–0011.

*MG 2041+1854*, at  $z=3.056$ , is a radio-loud quasar. The spectral index of this source is very close to the lower limit of our sample, which was imposed to separate the typically flat-spectrum quasars from the typically steeper-spectrum radio galaxies. The relatively bright ( $R \sim 20$ ) source is near the Galactic plane. Therefore, we took advantage of the good seeing conditions at Mauna Kea to take a short exposure spectrum of this source during twilight on a cirrusy night, though, consequently, the spectral fluxes are uncertain. The best image available for this source is from a 5s exposure through the guide camera at Keck (Fig. 1;  $0''.275 \text{ pix}^{-1}$ ). The field of view is smaller than for the other objects in Fig. 1 and the slit is visible; nevertheless, it is vastly superior to the poor-seeing Lick 3m image. The spectrum shows the typical broad lines of a quasar, with intervening  $\text{Mg II } \lambda \lambda 2800$  absorption systems apparent at  $z = 0.875, 1.469, 1.914$ , and  $1.946$ . This source is interesting in terms of being a moderately steep-spectrum, radio-loud quasar at  $z \gtrsim 3$ . Few such sources are in the literature and may be interesting in terms of unified models of extragalactic radio sources.

*MG 2058+0542*, at  $z=1.331$ , is typical of the sources discussed here. Narrow lines are visible with a faint red continuum, possibly suggestive of star light.



*MG 2109+0326*, at  $z=1.636$ , exhibits a slightly higher ionization spectrum than *MG 2058+0542*, or possibly reflects multiple ionization states, as indicated by the relatively strong [Ne IV]  $\lambda 2424$  emission line. An emission line galaxy at  $z = 0.790$  was also serendipitously discovered on the Keck spectrogram of this target.

*MG 2121+1839*, at  $z=1.861$ , shows neither the low-ionization C II]  $\lambda 2326$  nor the high ionization [Ne IV]  $\lambda 2424$  lines; the major features are C IV  $\lambda\lambda 1549$  and C III]  $\lambda 1909$ . Ly $\alpha$  has been detected for this object on the blue camera of the Kast Double Spectrograph of Lick Observatory. Keck/NIRC *K* band images of this target are presented in van Breugel et al. (1998) and reveal a relatively smooth morphology which is not aligned with the radio axis ( $PA_{4.8\text{GHz}} = 145^\circ$ , extended by  $6''3$ ). Serendipitous emission line galaxies at  $z = 0.353$  and  $z = 0.859$  were also discovered on the LRIS spectrogram.

*MG 2144+1928*, at  $z=3.592$ , is the highest redshift radio galaxy yet discovered in our MG sample. Its redshift was first measured at Lick Observatory and is mentioned in Spinrad et al. (1993). *MG 2144+1928* is an aligned radio galaxy with multiple components showing interesting velocity structure. Detailed discussion and analysis of the optical spectrum, as well as astrometry and a finding chart, is presented in Maxfield et al. (1998). Near-infrared observations of this galaxy are also presented in Armus et al. (1997) and van Breugel et al. (1998). Both the emission-line free *K'* image of van Breugel et al. (1998) and the narrow-band  $2.3\mu\text{m}$  image of Armus et al. (1997), selected to target the redshifted [O III]  $\lambda\lambda 4959, 5007$  doublet, show the host galaxy to be extended along the radio axis ( $PA_{4.8\text{GHz}} = 177^\circ$ , extended by  $8''5$ ).

*MG 2308+0336*, at  $z=2.457$ , is a high-redshift radio galaxy exhibiting a spectrogram indicative of mixed ionization state. Note that C II]  $\lambda 2326$ , the strongest of the carbon lines for this object, is quite broad. Ly $\alpha$  was also detected at Lick Observatory with the Kast Double Spectrograph. The optical counterpart consists of higher surface brightness core oriented at a position angle of  $137^\circ$ , with fainter emission evident to the south. The 4.8 GHz radio axis is aligned with the fainter emission ( $PA_{4.8\text{GHz}} = 175^\circ$ ) and is extended by  $3''$ .

#### 4. Emission Line Properties and Ionization State

In Fig. 3 we present a composite Keck/MG radio galaxy spectrum constructed from eleven of the spectra presented here, omitting the unfluxed spectra, the quasars, the extremely weak-lined *MG 1142+1338*, and *MG 1251+1104* whose spectrum is heavily affected by pattern noise. We also include *MG 1019+0534* and *MG 2144+1928*, the only previously published Keck spectra of MG radio galaxies (Dey, Spinrad, & Dickinson 1995; Maxfield et al. 1998), to maintain the integrity of the selection criterion: namely, we combine all Keck spectra of MG radio galaxies that we have amassed to date. This selection criteria ensures that we use only the highest signal-to-noise ratio data. The composite was constructed by shifting the individual spectra into their rest frame, rebinning to a common linear wavelength scale with  $2 \text{ \AA} \text{ pix}^{-1}$  resolution, and scaling the

spectra by the flux of the C III]  $\lambda 1909$  emission line. We select the C III]  $\lambda 1909$  feature since it is present in most of the spectra considered herein — in objects at both high and low redshift, as well as objects exhibiting high and low ionization spectra. We justify this algorithm in that our primary objective is to study the emission line properties of the MG sample; normalizing the spectra over a longer wavelength (line-free) range would give undue weight to the galaxies with the lowest continua. The current algorithm biases the continuum to the weakest-lined sources. Accordingly, we deemphasize conclusions drawn regarding the composite continuum. The red ends of the spectra were then trimmed to minimize contamination from the telluric OH features, and, in the case of MG 0311+1532, the effects of a nearby red star. The resultant vectors were then averaged. Only the spectrum of MG 2144+1928 did not overlap with the C III]  $\lambda 1909$  emission line. Instead, we normalized its spectrum to a preliminary composite comprising the other 12 galaxies using the C IV  $\lambda\lambda 1549$  doublet. The final spectrum is comparable to the composite radio galaxy spectrum constructed by McCarthy & Lawrence (1998; hereinafter McL98) primarily from 3C and MRC/1 Jy sources, which we also present in Fig. 3.

The emission line properties of the composite MG spectrum ( $\lambda\lambda 1100 - 2900 \text{ \AA}$ ) are presented in Table 6. We note that the emission line widths have not been corrected for the resolution of the spectrograph. For typical line widths of  $1100 \text{ km s}^{-1}$  observed at  $7500 \text{ \AA}$ , the deconvolution correction is  $\approx 75 \text{ km s}^{-1}$ . Comparisons to the emission line strengths determined from composite spectra of higher flux density radio galaxies (McL98), QSOs (Boyle 1990; Francis et al. 1991), Seyfert II nuclei (Ferland & Osterbrock 1986), the LINER nucleus of NGC 4579 (Barth et al. 1996), and models are presented in Table 2. All line profiles in the MG composite were fit with a simple Gaussian. This simple prescription overestimates the width of the doublet lines, most drastically for Mg II  $\lambda\lambda 2800$  whose rest-frame separation is  $7.2 \text{ \AA}$ . The typical FWHM for the remaining lines is  $900 - 1100 \text{ km sec}^{-1}$ , lower than that found by McL98 for their composite radio galaxy spectrum. Unlike McL98, we do not find that the FWHMs increase towards shorter wavelengths. However, the constituent galaxies in the McL98 composite stem from a much larger redshift range ( $0.16 < z < 3.13$ ), allowing a longer baseline composite spectrum ( $\lambda\lambda 800 - 5500 \text{ \AA}$ ). No strong trend is evident in their composite for the restricted wavelength range where both composites overlap. McL98 note that redshift correlates with [O II]  $\lambda 3727$  and [O III]  $\lambda\lambda 4959, 5007$  line width in 3CR galaxies, suggesting that the wavelength-line width trend in McL98 likely reflects a redshift-line width correlation, in the sense that higher redshift radio galaxies have broader emission lines. This is unlikely to be a selection effect, as the 3CR is nearly completely identified.

We measure an average restframe equivalent width of  $300 \text{ \AA}$  for the Ly $\alpha$  emission line in the Keck/MG radio galaxy sample. For comparison, from a sample of 28 radio galaxies with  $1.7 < z < 3.5$ , similar to the redshift range in the current sample, McCarthy (1993) finds a mean rest-frame  $W_\lambda(\text{Ly}\alpha)$  of  $295 \pm 188 \text{ \AA}$ . Radio-quiet, Lyman-break galaxies with Ly $\alpha$  in emission have a typical  $W_\lambda(\text{Ly}\alpha)$  of  $3 - 20 \text{ \AA}$  (Steidel et al. 1996). McL98 find that their composite radio galaxy spectrum has very strong Ly $\alpha$  relative to N V  $\lambda 1240$ , C IV  $\lambda\lambda 1549$ , and C III]  $\lambda 1909$ , as compared to other AGN. The MG composite, however, has much weaker Ly $\alpha$ , with line ratios more typical of

the other AGN in Table 2. Most likely the radio galaxy discrepancies stem from the small number of Ly $\alpha$  emitters in the composite spectra. The 3C/MRC composite Ly $\alpha$  comprises 7 galaxies, while the MG composite Ly $\alpha$  comprises only 3 galaxies, one of which is known to be underluminous in Ly $\alpha$ , likely due to dust absorption (MG 1019+0534, Dey, Spinrad, & Dickinson 1995). However, one could also imagine a Ly $\alpha$ –radio power dependency, similar to the known [O II]  $\lambda$ 3727 – 1.4 GHz radio power relation (McCarthy 1993), or that the MGs typically reside in dustier or more cold–gas–rich host galaxies.

At longer wavelengths, where the spectra are less affected by small number statistics, there are several significant differences between the radio galaxy composites. Most strikingly, the Mg II  $\lambda\lambda$ 2800 doublet is one of the most prominent lines in the MG composite, with Mg II  $\lambda\lambda$ 2800 / C III]  $\lambda$ 1909  $\sim$  1.2 and Ly $\alpha$  / Mg II  $\lambda\lambda$ 2800  $\sim$  4.4. In the 3C/MRC composite, however, the Mg II  $\lambda\lambda$ 2800 doublet is relatively weak, with Mg II  $\lambda\lambda$ 2800 / C III]  $\lambda$ 1909  $\sim$  0.4 and Ly $\alpha$  / Mg II  $\lambda\lambda$ 2800  $\sim$  41. The He II  $\lambda$ 1640 / Mg II  $\lambda\lambda$ 2800 line ratio also shows significant variation between the composite radio galaxy spectra: He II  $\lambda$ 1640 / Mg II  $\lambda\lambda$ 2800  $\sim$  0.8 for the MG sample, while He II  $\lambda$ 1640 / Mg II  $\lambda\lambda$ 2800  $\sim$  4.2 for the 3C/MRC composite. These strong discrepancies are difficult to interpret, though the MG line ratios are intriguingly more similar to those of LINERs and quasars than to the 3C/MRC composite radio galaxy or Seyfert IIs (see Table 2). We note that the Mg II  $\lambda\lambda$ 2800 line in the MG composite is composed from five spectra, suggesting that small number statistics may still be the source of these suggestive trends.

The strengths of the various ionization stages of carbon are a more useful diagnostic of the excitation mechanisms in active galaxies: selecting emission lines from the same element avoids metallicity dependencies, while the small wavelength separation of the lines considered makes the conclusions relatively insensitive to reddening. In Fig. 4 we plot C IV  $\lambda\lambda$ 1549 / C III]  $\lambda$ 1909 vs. C III]  $\lambda$ 1909 / C II]  $\lambda$ 2326 for individual galaxies in the MG sample, the composite spectra from Table 2, and the models described below. We find that the MG composite appears to be in a lower ionization state than the 3C/MRC composite, with carbon line ratios more comparable to the LINER nucleus of NGC 4579 than to the quasar composites. Again, an alternative explanation is that MGs typically reside in dustier galaxies than 3C/MRC sources. Unfortunately, the limited optical window and high redshift of the current sample deny us access to the line pairs commonly used for dust extinction measurements, such as H $\alpha$ /H $\beta$ , Ly $\alpha$ /H $\beta$ , and He II  $\lambda$ 1640/He II  $\lambda$ 4686. However, the strength of the Ly $\alpha$  line, which is quite sensitive to dust, implies that there is not an immense amount of reddening in the MG composite, while the dramatic change in the Mg II  $\lambda\lambda$ 2800 strength between the 3C/MRC composite and the MG composite suggests that there is a significant difference between the emission line regions in these two radio galaxy populations. Finally, the relatively high C II]  $\lambda$ 2326 / [Ne IV]  $\lambda$ 2424 ratio indicates that the MG composite is in a lower ionization state as compared to the higher radio power 3C/MRC composite, despite the [Ne IV]  $\lambda$ 2424 line residing redwards of the the carbon lines so that dust reddening alone can not explain the line ratio difference. This suggests that the ionization state of radio galaxies correlates with radio power. In a detailed study of lower redshift ( $z < 0.7$ ) southern 2 Jy radio sources, however, Tad-

hunter et al. (1998) find ionization state, as measured by the [O II]  $\lambda 3727$ /[O III]  $\lambda 5007$  ratio, does not correlate with radio power.

To test the hypothesis of a radio power—ionization state relation in high redshift radio galaxies, we have amassed a sample of 30 radio galaxies with published C IV  $\lambda\lambda 1549$  and C III]  $\lambda 1909$  fluxes from the literature. In Fig. 5 we plot C IV  $\lambda\lambda 1549$  / C III]  $\lambda 1909$  vs. rest-frame 1.4 GHz radio power. There is a slight tendency for the stronger radio sources to have larger C IV  $\lambda\lambda 1549$  / C III]  $\lambda 1909$  ratios, implying higher ionization states. To test the significance the correlation, we have calculated the nonparametric Spearman rank correlation coefficient,  $\rho$ , for this sample, and find a value of  $\rho = 0.340$ . Note that this statistic is independent of cosmology. The null hypothesis, that no correlation exists between radio power and ionization state can be marginally rejected: the probability of obtaining a rank correlation coefficient this high from a sample of 30 uncorrelated variables is 3.5%. If we restrict our analysis to the two larger data sets, i.e., the Keck/MG and ultra-steep source (USS) samples, then  $\rho = 0.445$  for a sample of 25 sources. The probability of obtaining a rank correlation coefficient this high from a sample of 25 uncorrelated variables is 1.5%, implying that the correlation is significant. We consider these statistical arguments suggestive, but not conclusive, of a radio power—ionization state correlation in the UV spectra of high-redshift radio galaxies. Insufficient sources with both He II  $\lambda 1640$  and Mg II  $\lambda\lambda 2800$  well-detected prevented a similar analysis to be done with the He II  $\lambda 1640$  / Mg II  $\lambda\lambda 2800$  ratio.

We have computed simple, single-zone photoionization models using CLOUDY (Ferland 1996). The purpose of this exercise is not to fabricate a definitive model of the radio galaxy spectrum, but rather to demonstrate that a simple low density gas photoionization model can reproduce the overall character of the spectrum and compare the best-fit parameters with those derived for the 3C/MRC composite. Following McL98, our calculations were made for an ionization bounded slab of gas with a constant density of  $n_e = 100 \text{ cm}^{-3}$  illuminated by a power-law spectrum of ionizing radiation,  $F_\nu \propto \nu^{-\alpha}$ . We calculated models with a range of spectral index,  $\alpha$ , and ionization parameter,  $U$ . For reference, McL98 found that  $\alpha = 1.5$  and  $\log U = -1.8$  provided the best fit to the composite 3C/MRC spectrum.

We find that the carbon line diagnostics are not well-reproduced by these simple models. For example, the best-fit CLOUDY model of McL98 is represented by an asterisk in Fig. 4. Though this model does a reasonable job at reproducing the overall character of the 3C/MRC emission line spectrum, the C III]  $\lambda 1909$  / C II]  $\lambda 2326$  ratio is much higher in the model than in the composite spectrum. Fig. 2d of Allen et al. (1998) is also enlightening: for a given C IV  $\lambda\lambda 1549$  / C III]  $\lambda 1909$  ratio, the C II]  $\lambda 2326$  emission line is again too strong in the comparison AGN spectra to be fit by simple single-zone photoionization models. Photoionization models which incorporate both optically thick (ionization bounded) clouds and optically thin (matter bounded) clouds, as described in Binnette et al. (1996), are capable of reproducing the observed carbon line diagnostics, as are the shock models of Dopita & Sutherland (1996), implying that (the MG) radio galaxies are more complicated than our basic model. Investigations also reveal that the high equivalent width Mg II  $\lambda\lambda 2800$  line is also difficult to reproduce with the simple model: for  $1.0 < \alpha < 1.5$  and

$-1.0 < \log U < -2.0$ , no model is capable of reproducing the Mg II  $\lambda\lambda 2800$  / C III]  $\lambda 1909$  ratio we find in the MG composite radio galaxy spectrum, indicating that shocks and/or more complicated photoionization scenarios are necessary to explain the emission line spectra of these galaxies.

## 5. Conclusions

We present optical identifications, finding charts, and spectra for seventeen new high-redshift radio sources selected from the MG 5 GHz survey. We select targets of moderately steep spectral index to preferentially observe radio galaxies, and, indeed, fifteen of the seventeen sources discussed herein are radio galaxies. The remaining two sources are moderately steep-spectrum, radio-loud quasars which may be important in terms of unified models of extragalactic radio sources. The spectra were all taken at the W.M. Keck Telescopes and are representative of the fainter MG identifications attempted thus far, with typical  $R$  magnitudes of 23 – 24.

We construct a composite MG radio galaxy spectrum and compare it with the higher-radio power composite 3C/MRC radio galaxy spectrum of McL98. We find that the MG radio galaxies typically exhibit lower ionization state spectra than the 3C/MRC radio galaxies. The Mg II  $\lambda\lambda 2800$  emission line is extremely strong in the MG composite relative to the other rest-frame UV emission lines, with Mg II  $\lambda\lambda 2800$  / C III]  $\lambda 1909 \sim 1.5$  and Mg II  $\lambda\lambda 2800$  / Ly $\alpha \sim 0.3$ . Extensive modeling with single-zone photoionization models are incapable of reproducing the high Mg II  $\lambda\lambda 2800$  / C III]  $\lambda 1909$  ratio, indicating that shocks and/or more complicated photoionization scenarios are producing the emission line spectra of these distant radio galaxies.

We have amassed a large sample of high-redshift radio galaxies with published C IV  $\lambda\lambda 1549$  and C III]  $\lambda 1909$  line strengths. Comparing the C IV  $\lambda\lambda 1549$  / C III]  $\lambda 1909$  ratio to the rest-frame 1.4 GHz radio power, we find evidence for a correlation between ionization state and radio power. A likely interpretation is that the more powerful radio sources are in an active phase when the central engine is emitting more flux across the electromagnetic spectrum with the augmented UV flux leading to higher ionization state spectra. As we progress from the strongest radio sources to weaker sources, we find the emission line strengths attenuate, the ionization state of the emission line region diminishes, and the stellar populations apparently become more dominant. This last effect is seen both in the diminished alignment affect for weak radio sources and the discovery of several weak radio sources at moderate redshift whose spectra are devoid of the UV emission lines that dominate most radio galaxy spectra (e.g., Spinrad et al. 1997). An alternative explanation is to invoke multiple emission line regions whose relative contributions vary with radio power.

The high-redshift radio galaxies discussed herein are faint, and the radio power-line strength correlation implies that long integrations with the new generation of large aperture telescopes is necessary to measure the emission line strengths and redshifts of these sources. High-redshift radio galaxies from a range of radio flux density will be the key to further investigations of the ionization state-radio power relation.

We are very grateful to B. Burke and Sam Conner at MIT for introducing us to the MG sample and for supplying much of the astrometry for our candidate subset. We thank Aaron Barth, Wil van Breugel, and Pat McCarthy for valuable discussion and useful comments on the manuscript. We acknowledge Chuck Steidel for graciously obtaining the MDM images, Marc Davis and Steve Zepf for obtaining the spectra of MG 0422+0816 and MG 0511+0143, Marc Davis and Jeffrey Newman for obtaining the spectra of MG 0148+1028 and MG 0308+0720, and Pat McCarthy for providing the composite 3C/MRC radio galaxy spectrum. We thank Brian McLeod who has imaged a subset of the MG sample in the K band and T. Bida, W. Wack and J. Aycock for invaluable help during our Keck runs. The authors also gratefully acknowledge the referee, Rogier Windhorst, for useful comments. DS acknowledges support from IGPP grant 99–AP026, AD acknowledges the support of NASA grant HF–01089.01–97A and partial support from a postdoctoral research fellowship at NOAO, HS acknowledges support from NSF grant AST 95–28536. DS, AD, and DS acknowledge Peet for invaluable help at the observatories and for facilitating coherent discussion.

## REFERENCES

- Allen, M.G., Dopita, M.A., & Tsvetanov, Zl. 1998, *ApJ*, 493, 571
- Allington-Smith, J.R. 1982, *MNRAS*, 199, 611
- Armus, L., Soifer, B.T., Murphy, T.W., Jr., Neugebauer, G., Evans, A.S., & Matthews, K. 1997, *ApJ*, 495, 276
- Barth, A.J., Reichert, G.A., Filippenko, A.V., Ho, L.C., Shields, J.C., Mushotzky, R.F., & Puchnarewicz, E.M. 1996, *AJ*, 112, 1829
- Becker, R., Whiter, R., & Edwards, A. 1991, *ApJS*, 75, 1
- Bennett, C.L., Lawrence, C.R., Burke, B.F., Hewitt, J.N., & Mahoney, J. 1986, *ApJS*, 61, 1
- Binette, L, Wilson, A.S., & Storchi-Bergmann, T. 1996, *A&A*, 312, 365
- Blumenthal, G., & Miley, G.K. 1979, *A&A*, 80, 13
- Boyle, B.J. 1990, *MNRAS*, 243, 231
- Brotherton, M.S., Wills, B.J., Francis, P.J., & Steidel, C.S. 1994, *ApJ*, 430, 495
- Burstein, D. & Heiles, C. 1982, *AJ*, 87, 1165
- Cardelli, J.A., Clayton, C.C., & Mathis, J.S. 1989, *ApJ*, 345, 245
- Chambers, R.C., Miley, G.K., & van Breugel, W. 1987, *Nature*, 329, 604
- Cimatti, A., di Serego Alighieri, S., Vernet, J., Cohen, M. & Fosbury, R.A.E. 1998, *ApJ*, 499, 21
- Dey, A., Spinrad, H., Dickinson, M. 1995, *ApJ*, 440, 515
- Dey, A., van Breugel, W., Vacca, W., & Antonucci, R. 1997, *ApJ*, 490, 698
- Dey, A., et al. 1998, in preparation

- Dickinson, M., et al. 1996, in *Fresh Views of Elliptical Galaxies*, ed. Buzzoni, Renzini, & Serrano (ASP Conf. Ser., 86), 283
- Djorgovski, S. 1985, *PASP*, 97, 1119
- Dopita, M.A. & Sutherland, R.S. 1996, *ApJS*, 102, 161
- Dunlop, J.S. & Peacock, J. 1991, *MNRAS*, 263, 936
- Dunlop, J.S., Peacock, J., Spinrad, H., Dey, A., Jimenez, R., Stern, D., & Windhorst, R. 1996, *Nature*, 381, 581
- Eales, S. & Rawlings, S. 1993, *ApJ*, 411, 67
- Ferland, G.J. 1996, *Hazy: A Brief Introduction to CLOUDY*, Univ. of Kentucky Dept. of Phys. and Astron. Internal Report
- Ferland, G.J. & Osterbrock, D.E. 1986, *ApJ*, 300, 658
- Filippenko, A.V. 1982, *PASP*, 94, 715
- Francis, P., Hewett, P.C., Foltz, C.B., Chaffee, F.H., Weymann, R.J., & Morris, S.L. 1991, *ApJ*, 373, 465
- Gregory, P.C. & Condon, J.J. 1991, *ApJS*, 75, 1011
- Griffiths, M., Wright, M., Burke, B., & Ekers, R. 1995, *ApJS*, 97, 347
- Hales, S.E.G., Baldwin, J.E., & Warner, P.J. 1993, *MNRAS*, 234, 919
- Knopp, G.P. & Chambers, K.C. 1997, *ApJS*, 109, 367
- Lacy, M., et al. 1994, *MNRAS*, 271, 504
- Lawrence, C.R., Readhead, A.C.S., Moffet, A.T., & Birkinshaw, M. 1986, *ApJS*, 61, 105
- Lowenthal, J. et al. 1997, *ApJ*, 481, 673
- Massey, P., Strobel, K., Barnes, J.V., & Anderson, E. 1988, *ApJ*, 328, 315
- Massey, P. & Gronwall, C. 1990, *ApJ*, 358, 344
- Maxfield, L., et al. 1998, in preparation
- McCarthy, P., van Breugel, W., Spinrad, H., & Djorgovski, S. 1987, *ApJ*, 321, L29
- McCarthy, P., Spinrad, H., Dickinson, M., van Breugel, W., Liebert, J., Djorgovski, S., & Eisenhardt, P. 1990, *ApJ*, 365, 487
- McCarthy, P. 1993, *ARA&A*, 31, 639
- McCarthy, P., Kapahi, V.K., van Breugel, W., Persson, S.E., Athreya, R., & Subrahmanya, C.R. 1996, *ApJS*, 107, 19
- McCarthy, P. & Lawrence, C.R. 1998, in preparation (McL98)
- Miller, J.S. & Stone, R.P.S. 1994, *Lick Obs. Tech. Rep.* 66
- Neuschaefer, L.W. & Windhorst, R.A. 1995, *ApJS*, 96, 371

- Oke, J.B., et al. 1995, *PASP*, 107, 375
- Rawlings, S. & Saunders, R. 1991, *Nature*, 349, 138
- Rawlings, S., Lacy, M., Blundell, K. M., Eales, S. A., Bunker, A. J., & Garrington, S. T. 1996, *Nature*, 383, 502
- Röttgering, H.J.A., Lacy, M., Miley, G.K., Chambers, K.C., & Saunders, R. 1994, *A&A*, 108, 79
- Spinrad, H. & Djorgovski, S. 1987, in *Observational Cosmology*, ed. A. Hewitt, G. Burbridge, & L.Z. Fang (IAU Symp. 124), 129
- Spinrad, H., Dickinson, M., Schlegel, D., & Gonzalez, R. 1993, in *Observational Cosmology*, ed. G. Chincarini, A. Iovino, & D. Maccagni (ASP Conf. Ser., 51), 585
- Spinrad, H., Dey, A., & Graham, J.R. 1995, *ApJ*, 438, L51
- Spinrad, H., Dey, A., Stern, D., Dunlop, J., Peacock, J., Jimenez, R., & Windhorst, R. 1997, *ApJ*, 484, 581
- Spinrad, H., Dey, A., Stern, & Bunker, A. 1998, in *Proc. Know Colloq.*, ed. H. Röttgering, in press
- Steidel, C.C., Giavalisco, M., Pettini, M., Dickinson, M., & Adelberger K.L. 1996, *ApJ*, 462, L17
- Stern, D., Spinrad, H., Dickinson, M. 1996, *AJ*, 111, 102
- Stern, D., Spinrad, H., Dey, A., Dickinson, M., & Schlegel, D. 1997, in *The HST and the High-Redshift Universe*, ed. N. Tanvir, A. Aragon-Salamanca, & J. Wall (37th Herstmonceux), 413.
- Tadhunter, C.N., Morganti, R., Robinson, A., Dickson, R., Villar-Martin, M., & Fosbury, R.A.E. 1998, *MNRAS*, in press
- Thompson, D., Djorgovski, S., Vigotti, M., & GruEFF, G. 1994 *AJ*, 108, 828
- van Breugel, W., Stanford, S., Spinrad, H., Stern, D., & Graham, J.R. 1998, *ApJ*, 502, 614
- van Ojik, R. 1995, PhD thesis, Rijksuniversiteit te Leiden
- Vigotti, M., GruEFF, G., Perley, R., Clark, B., & Bridle, A. 1989, *AJ*, 98, 419



Table 1. Journal of the observations.

Source	Observation Type <sup>†</sup>	Observation Date	Telescope	Exposure (seconds)
MG 0018+0940	I	1995 Sep 01	Keck	600
	S	1995 Sep 01	Keck	1500
MG 0046+1102	I	1995 Sep 01	Keck	1050
	S	1995 Sep 01	Keck	3000
MG 0122+1923	I	1995 Sep 01	Keck	600
	S	1997 Sep 12	Keck	2400
MG 0148+1028	I	1996 Oct 15	Lick	1260
	S	1997 Dec 23	Keck	1800
MG 0308+0720	I	1996 Oct 15	Lick	600
	S	1997 Dec 23	Keck	1800
MG 0311+1532	I	1994 Jan 11	MDM	600
	S	1995 Aug 31	Keck	3600
MG 0422+0816	I	1992 Nov 25	Lick	200
	S	1995 Oct 25	Keck	1800
MG 0511+0143	I	1992 Nov 25	Lick	1500
	S	1995 Oct 25	Keck	1800
MG 1142+1338	I	1994 Apr 07	MDM	1800
	S	1995 Feb 03	Keck	2400
MG 1251+1104	I	1995 Mar 14	Keck	1200
	S	1995 Mar 15	Keck	4500
MG 1401+0921	I	1997 Jul 01	Keck	900
	S	1997 Jul 02	Keck	2400
MG 2037–0011	I	1994 Sep 30	MDM	1500
	S	1995 Jul 23	Keck	3600
	S	1995 Jul 24	Keck	3600
	S	1995 Aug 31	Keck	3600
MG 2041+1854	S	1996 Jun 16	Keck	300
MG 2058+0542	I	1992 Aug 01	Lick	1400
	I	1993 Aug 17	Lick	1500
	S	1994 Jul 10	Keck	3000
MG 2109+0326	I	1993 Sep 14	Lick	1100
	S	1994 Jul 09	Keck	6550
MG 2121+1839	I	1992 Aug 01	Lick	1200
	S	1994 Jun 10	Keck	4500
MG 2308+0336	I	1995 Jul 25	Keck	600

Table 1—Continued

Source	Observation Type <sup>†</sup>	Observation Date	Telescope	Exposure (seconds)
	S	1995 Jul 23	Keck	2400

<sup>†</sup>I: imaging; S: spectroscopy.

Table 2. Astrometric data.

Source		$\alpha_{2000}$	$\delta_{2000}$
MG 0018+0940	R	00 18 55.23	+09 40 06.9
	O	00 18 55.24	+09 40 06.8
	A	00 18 53.93	+09 40 24.6
MG 0046+1102	R	00 46 41.40	+11 02 52.6
	O	00 46 41.38	+11 02 52.5
	A	00 46 43.88	+11 02 33.3
MG 0122+1923	R	01 22 29.95	+19 23 39.1
	O	01 22 29.90	+19 23 38.6
	A	01 22 31.27	+19 24 10.2
MG 0148+1028	R	01 48 28.85	+10 28 21.3
	O	01 48 28.83	+10 28 22.0
	A	01 48 26.23	+10 27 52.3
MG 0308+0720	R	03 08 41.90	+07 20 44.3
	O	03 08 41.98	+07 20 44.9
	A	03 08 40.35	+07 21 18.3
MG 0311+1532	R	03 11 56.89	+15 32 54.8
	O	03 11 56.83	+15 32 55.4
	A	03 11 54.52	+15 32 49.7
MG 0422+0816	R	04 22 24.00	+08 16 19.2
	O	04 22 23.97	+08 16 18.7
	A	04 22 23.95	+08 16 31.2
MG 0511+0143	R	05 11 04.77	+01 41 57.8
	O	05 11 04.76	+01 42 00.3
	A	05 11 02.89	+01 41 54.7
MG 1142+1338	R	11 42 23.6	+13 38 01.3
	O	11 42 23.69	+13 38 01.4
	A	11 42 22.80	+13 37 51.9
MG 1251+1104	R	12 51 00.02	+11 04 19.9
	O	12 51 00.02	+11 04 21.6
	A	12 50 58.67	+11 04 45.7
MG 1401+0921	R	14 01 18.3	+09 21 23.7
	O	14 01 18.50	+09 21 21.2
	A	14 01 16.66	+09 20 51.5
MG 2037–0011	R	20 37 13.41	–00 10 58.5
	O	20 37 13.41	–00 10 58.5
	A	20 37 12.90	–00 10 56.9

Table 2—Continued

Source		$\alpha_{2000}$	$\delta_{2000}$
MG 2041+1854	R	20 41 24.2	+18 55 02.0
	O	20 41 24.09	+18 55 00.9
	A	20 41 25.20	+18 55 11.1
MG 2058+0542	R	20 58 28.95	+05 42 51.0
	O	20 58 28.82	+05 42 50.7
	A	20 58 30.13	+05 42 43.7
MG 2109+0326	R	21 09 21.71	+03 26 52.7
	O	21 09 21.80	+03 26 51.6
	A	21 09 20.93	+03 26 30.8
MG 2121+1839	R	21 21 25.48	+18 39 08.7
	O	21 21 25.48	+18 39 09.0
	A	21 21 25.35	+18 38 53.6
MG 2308+0336	R	23 08 25.0	+03 37 03.0
	O	23 08 25.15	+03 37 03.6
	A	23 08 26.07	+03 36 22.3

Note. — R: radio source; O: optical counterpart;  
A: offset star.

Table 3. Imaging Properties of the sample.

Source	$z$	$R$ (mag)	$4 \times E_{B-V}$	$S_{4.8\text{GHz}}$ (mJy)	$\alpha_{1.4\text{GHz}}^{4.8\text{GHz}}$	Size ( $''$ )	PA ( $^\circ$ )	$\log L_{4.8\text{GHz}}$ ( $\text{erg s}^{-1} \text{ Hz}^{-1}$ )
MG 0018+0940	1.586	23.0	0.237	132	1.08	0.0	...	34.70
MG 0046+1102	1.813	23.1	0.209	74	1.07	0.0	...	34.61
MG 0122+1923	1.595	23.3	0.105	134	1.06	0.0	...	34.70
MG 0148+1028	2.845	21.4	0.157	176	0.71	0.0	...	35.39
MG 0308+0720	2.975	21.1	0.801	164	0.95	0.0	...	35.56
MG 0311+1532	1.986	23.6	0.405	62	1.21	5.1	161	34.72
MG 0422+0816	0.294	20: <sup>†</sup>	0.721	68	1.06	0.0	...	32.53
MG 0511+0143	0.596	22: <sup>†</sup>	0.393	98	1.06	3.9	171	33.4 2
MG 1019+0534	2.765	23.7	0.037	100	1.22	1.3	103	35.40
MG 1142+1338	1.279	23.9	0.093	149	1.03	0.0	...	34.46
MG 1251+1104	2.322	24:	0.000	62	1.21	0.0	...	34.94
MG 1401+0921	2.093	23.3	0.013	92	0.89	3.5	138	34.81
MG 2037–0011	1.512	24.8	0.397	119	1.03	0.0	...	34.57
MG 2041+1854	3.056	20: <sup>†</sup>	0.441	217	0.76	0.0	...	35. 10
MG 2058+0542	1.381	23.7	0.425	283	1.19:	0.0	...	34.90
MG 2109+0326	1.634	22.0	0.281	119	0.75	0.0	...	34.55
MG 2121+1839	1.860	22.7	0.341	69	1.09	6.3	145	34.63
MG 2144+1928	3.592	23.5:	0.449	58	1.54	8.5	177	35.76
MG 2308+0336	2.457	23:	0.173	148	0.85	3.0	175	35.20

<sup>†</sup>estimated from non-photometric conditions

Note. — Keck magnitudes are in  $2''$  apertures, MDM magnitudes are in  $2''.5$  apertures, and Lick magnitudes are in  $4''$  apertures. Keck and MDM images are through an  $R$  filter, while Lick observations are through the Spinrad night-sky filter,  $R_S$  (Djorgovski 1986). We assume  $H_0 = 50 \text{ km s}^{-1} \text{ Mpc}^{-1}$ ,  $q_0 = 0$  to calculate the radio powers. Uncertain numbers are indicated with a colon. Reddening corrections have only been applied to the spectroscopy.

Table 4. 4.85 GHz Flux Densities for the Sample

Source	1986	Becker et al. 1991 <sup>†</sup>	Gregory & Condon 1991	Griffiths et al. 1995
MG 0018+0940	132	156	159 ± 22	190 ± 14
MG 0046+1102	74	98	100 ± 15	...
MG 0122+1923	134	115	117 ± 16	...
MG 0148+1028	176	192	193 ± 27	...
MG 0308+0720	164	161	165 ± 23	213 ± 15
MG 0311+1532	62	53	54 ± 9	...
MG 0422+0816	68	113	116 ± 17	102 ± 12
MG 0511+0143	98	104	107 ± 16	102 ± 12
MG 1019+0534	115	115	132 ± 19	100 ± 12
MG 1142+1338	149	125	127 ± 18	...
MG 1251+1104	62	...	...	...
MG 1401+0921	92	89	92 ± 14	66 ± 11
MG 2037–0011	119	114	...	179 ± 14
MG 2041+1854	217	173	178 ± 24	...
MG 2058+0542	283	424	427 ± 59	356 ± 21
MG 2109+0326	119	81	86 ± 14	75 ± 11
MG 2121+1839	69	61	65 ± 10	...
MG 2144+1928	58	71	76 ± 11	...
MG 2308+0336	148	158	163 ± 23	160 ± 13

<sup>†</sup>Becker et al. 1991 report a 15% error on all measurements.

Note. — All flux densities measured in mJy. The 1986 flux densities for MG 0511+0143 and MG 2308+0336 are from Bennett et al. (1986); the remaining 1986 flux densities are from Lawrence et al. (1986).

Table 5. Observed emission lines.

Source	Line ID	$\lambda_{\text{obs}}$ (Å)	$f \times 10^{-17}$ (erg cm <sup>-2</sup> s <sup>-1</sup> )	$W_{\lambda}$ (Å)	$z$
MG 0018+0940	C IV 1549	4004.4	8.1	145	1.584
	He II 1640	4243.7	4.2	92	1.588
	C III] 1909	4934.6	8.7	161	1.585
	C II] 2326	6016.7	6.5	137	1.587
	[Ne IV] 3426	6263.8	3.1	90	1.584
	Mg II 2798	7236.7	8.8	227	1.585
	He II 3203	8291.3	3.1	64	1.589
MG 0046+1102	C IV 1549	4357.2	6.5	99	1.812
	He II 1640	4615.8	5.5	83	1.814
	C III] 1909	5366.5	7.9	124	1.811
	C II] 2326	6542.6	7.4	120	1.813
	[Ne IV] 3426	6813.2	1.9	29	1.811
	O II 2470	6947.5	2.0	30	1.813
	Mg II 2798	7875.6	11.8	176	1.814
MG 0122+1928	C IV $\lambda\lambda$ 1549	4033.9	3.2	54	1.604
	He II $\lambda$ 1640	4262.9	3.8	81	1.599
	C III] $\lambda$ 1909	4958.0	3.2	60	1.597
	C II] $\lambda$ 2326	6047.3	2.3	64	1.600
	Mg II $\lambda\lambda$ 2800	7273.3	3.1	77	1.598
MG 0148+1028	Ly $\alpha$	4676.1	101.8	116	2.845
	C IV $\lambda\lambda$ 1549	5965.3	116.3	128	2.851
	He II $\lambda$ 1640	6304.9	26.0	29	2.844
	O III] $\lambda\lambda$ 1663	6400.8	8.4	9	2.849
	C III] $\lambda$ 1909	7333.8	57.8	67	2.842
MG 0308+0720	Ly $\alpha$	4858.3	181.8	71	2.995
	N V $\lambda$ 1240	4905.8	529.3	221	2.956
	Si/0 II $\lambda\lambda$ 1400	5587.0	56.3	26	2.991
	C IV $\lambda\lambda$ 1549	6162.9	155.9	75	2.979
	C III] $\lambda$ 1909	7565.2	69.8	39	2.963
MG 0311+1532	C IV $\lambda\lambda$ 1549	4634.1	3.4	160	1.991
	He II $\lambda$ 1640	4903.5	2.0	103	1.990
	C III] $\lambda$ 1909	5703.8	2.1	97	1.988
	C II] $\lambda$ 2326	...	...	...	...
	[Ne IV] $\lambda$ 2424	7239.3	1.1	50	1.988
MG 1019+0534	Ly $\alpha$	4584.3	8.4	268	2.770

Table 5—Continued

Source	Line ID	$\lambda_{\text{obs}}$ ( $\text{\AA}$ )	$f \times 10^{-17}$ ( $\text{erg cm}^{-2} \text{s}^{-1}$ )	$W_{\lambda}$ ( $\text{\AA}$ )	$z$
	N V $\lambda$ 1240	4664.8	2.3	66	2.762
	C IV $\lambda\lambda$ 1549	5838.9	10.4	257	2.769
	He II $\lambda$ 1640	6174.9	8.5	170	2.765
	C III] $\lambda$ 1909	7179.6	4.9	93	2.760
MG 1142+1338	C III] $\lambda$ 1909	...	<3.0	...	...
	C II] 2326	...	<1.6	...	...
	[Ne V] 3426	7783.6	5.4	112	1.272
	[O II] 3727	8495.1	13.6	232	1.279
MG 1251+1104	Ly $\alpha$	4040.5	23.1	148	2.324
	C IV 1549	5148.4	3.0	...	2.324
	He II 1640	5453.2	3.0	...	2.325
	C III] 1909	6326.7	5.2	298	2.314
	C II] 2326	...	<4.5	...	...
MG 1401+0921	C IV 1549	4793.9	4.1	165	2.095
	He II 1640	5072.8	5.0	171	2.093
	C III] 1909	5901.1	3.4	83	2.091
	C II] 2326	7187.2	1.7	89	2.090
	[Ne IV] 2423	7521.8	2.9	121	2.104
MG 2037–0011	C III] 1909	4782.2	4.4	123	1.505
	C II] 2326	5843.5	1.0	39	1.512
	[Ne IV] 2424	6093.9	1.0	43	1.514
MG 2041+1854	Ly $\alpha$	4986	788.5	141	3.100
	Si IV] 1400	5695:	130.8	28	3.05:
	C IV 1549	6283	417.8	54	3.056
	C III] 1909	7785:	68.3	25	3.08:
MG 2058+0542	C III] 1909	4541.3	7.1	152	1.379
	C II] 2326	5537.6	4.1	120	1.381
	Mg II 2798	6667.0	6.6	206	1.381
	[Ne IV] 2423	5769.6	1.3	45	1.380
	[Ne V] 3426	...	<2.0	...	...
	[O II] 3727	8877.4	12.0	240	1.382
MG 2109+0326	C IV 1549	...	<1.0	...	...
	He II 1640	4323.7	3.2	148	1.636
	C III] 1909	5029.4	2.1	105	1.635
	C II] 2326	6136.6	2.3	110	1.638



Fig. 1.— Finding charts for the new identifications. Fields are 1.5 arcmin square, with north at the top and east to the left. Identifications are indicated with two dashes. The offset star in each field is marked with a capital A. Note that for MG 2308+0336 no bright stars are within the field-of-view; instead an offset galaxy is indicated.

Table 5—Continued

Source	Line ID	$\lambda_{\text{obs}}$ (Å)	$f \times 10^{-17}$ (erg cm <sup>-2</sup> s <sup>-1</sup> )	$W_{\lambda}$ (Å)	$z$
MG 2121+1839	[Ne IV] 2423	6386.8	1.3	40	1.635
	Mg II 2798	7364.9	0.9	22:	1.631
	C IV 1549	4431.7	5.3	134	1.861
	He II 1640	4709.3	1.4	28	1.872
	C III] 1909	5462.6	2.4	47	1.861
	C II] 2326	6675:	1.5:	45:	1.869
	[Ne V] 3426	...	<1.0	...	...
MG 2144+1928	Mg II 2798	...	<0.5	...	...
	Ly $\alpha$	5586.8	61.5	686	3.596
	C IV 1549	7112.2	5.8	234	3.589
MG 2308+0336	He II 1640	7534.4	3.5	362	3.594
	Ly $\alpha$	4209.2	29.3	284	2.462
	N V 1240	4288.2	5.7	118	2.458
	C IV 1549	5357.9	6.3	91	2.458
	He II 1640	5669.1	3.9	78	2.457
	C III] 1909	6589.1	4.5	110	2.452
C II] 2326	8036.9	8.3	412	2.455	

Note. — Uncertain measurements are indicated with a colon. Values for MG 1019+0534 are from Dey, Spinrad, & Dickinson 1995. Values for MG 2144+1928 are from Maxfield et al. 1998.

Table 6. Composite Keck/MG radio galaxy spectrum.

Line	$\lambda$ ( $\text{\AA}$ )	Flux Density	$W_\lambda$ ( $\text{\AA}$ )	FWHM ( $\text{km s}^{-1}$ )	Comment
Ly $\alpha$	1216	515	116	1130	
Ly $\alpha^\dagger$	1216	606	106	1140	
N V	1240	53	13	1420	
C IV	1549	131	31	1540	doublet
He II	1640	94	23	1150	
C III]	1909	100	28	1260	
C II]	2326	83	30	1720	
[Ne IV]	2424	49	16	1780	
[O II]	2470	17	5	930	
Mg II	2800	116	42	2100	doublet
[O II]	3727	188	142	1060	

<sup>†</sup>Composite composed without MG 1019+0534, a dusty radio galaxy known to be underluminous in Ly $\alpha$  (Dey, Spinrad, & Dickinson 1995).

Note. — All line strengths measured relative to C III]  $\lambda$ 1909, whose flux has been arbitrarily scaled to 100.

Table 2. Comparisons with Other AGN and Models — Normalized Line Flux Densities.

Line	$\lambda$ ( $\text{\AA}$ )	HzRG MG	HzRG 3C/MRC	Seyfert II	LINER NGC 4579	QSO Boyle	QSO Francis
Ly $\alpha$	1216	515 <sup>†</sup>	1766	1000	239	485	253
N V	1240	53	88	...	...	128	...
C IV	1549	131	207	218	81	224	217
He II	1640	94	181	37	4	26	62
C III]	1909	100	100	100	100	100	100
C II]	2326	83	52	...	32	19	20
[Ne IV]	2424	49	51	...	<8	...	8
[O II]	2470	17	23	...	7	...	...
Mg II	2800	116	43	33	113	113	117
[O II]	3727	188	207	103	...	...	0.3

<sup>†</sup>When composite is created without MG 1019+0534, a dusty radio galaxy known to be underluminous in Ly $\alpha$ (Dey, Spinrad, & Dickinson 1995), the value of  $100 \times \text{Ly}\alpha / \text{C III] } \lambda 1909 = 606$ .

Note. — All line strengths are measured relative to C III]. MG high-redshift radio galaxy (HzRG) composite derives from the current work, 3C/MRC HzRG composite is from McL98, Seyfert II composite is from Ferland & Osterbrock (1986), UV spectrum of LINER nucleus of NGC 4579 is from Barth et al. (1996), and QSO composites are from Boyle (1990) and Francis et al. (1991).

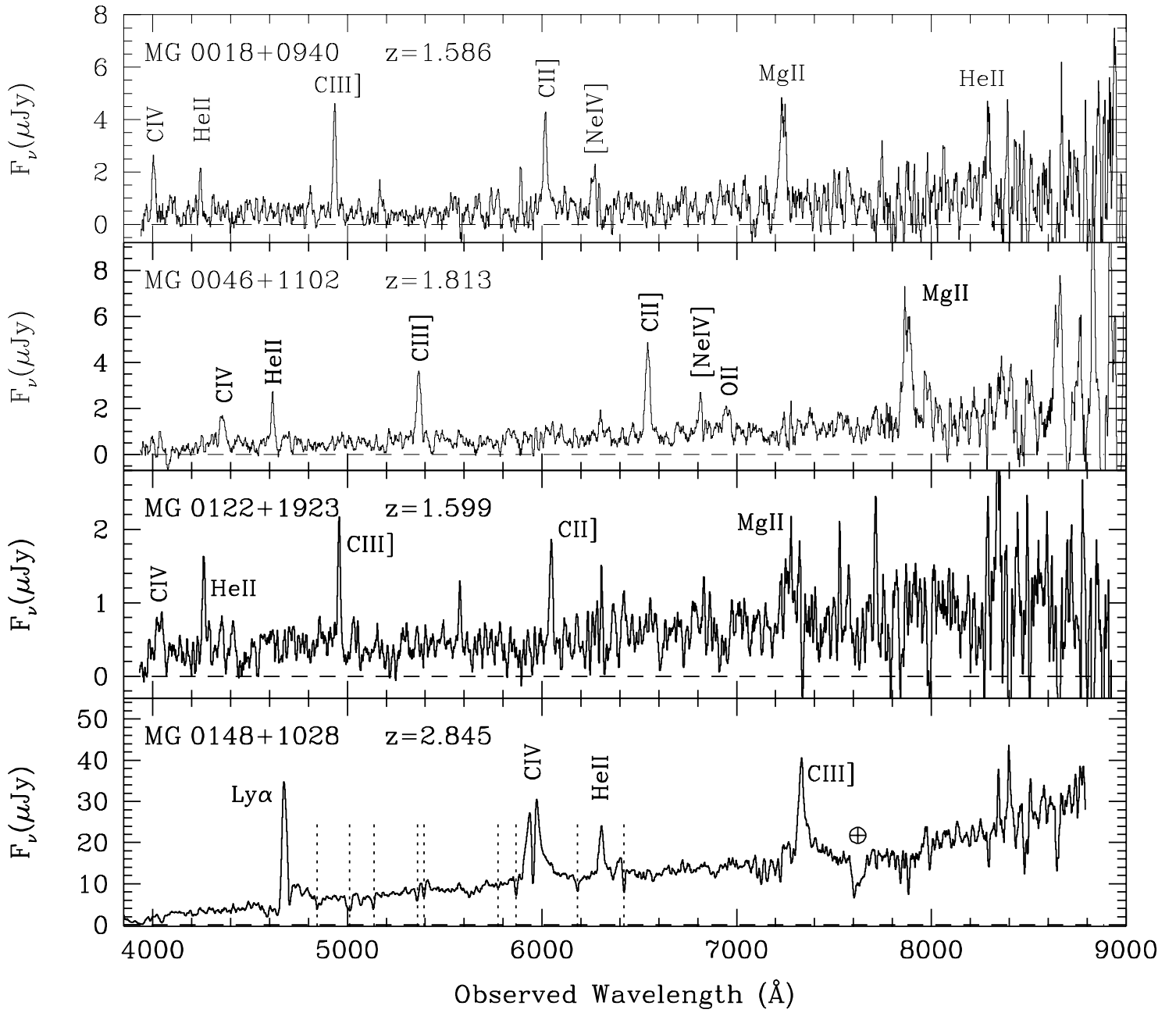
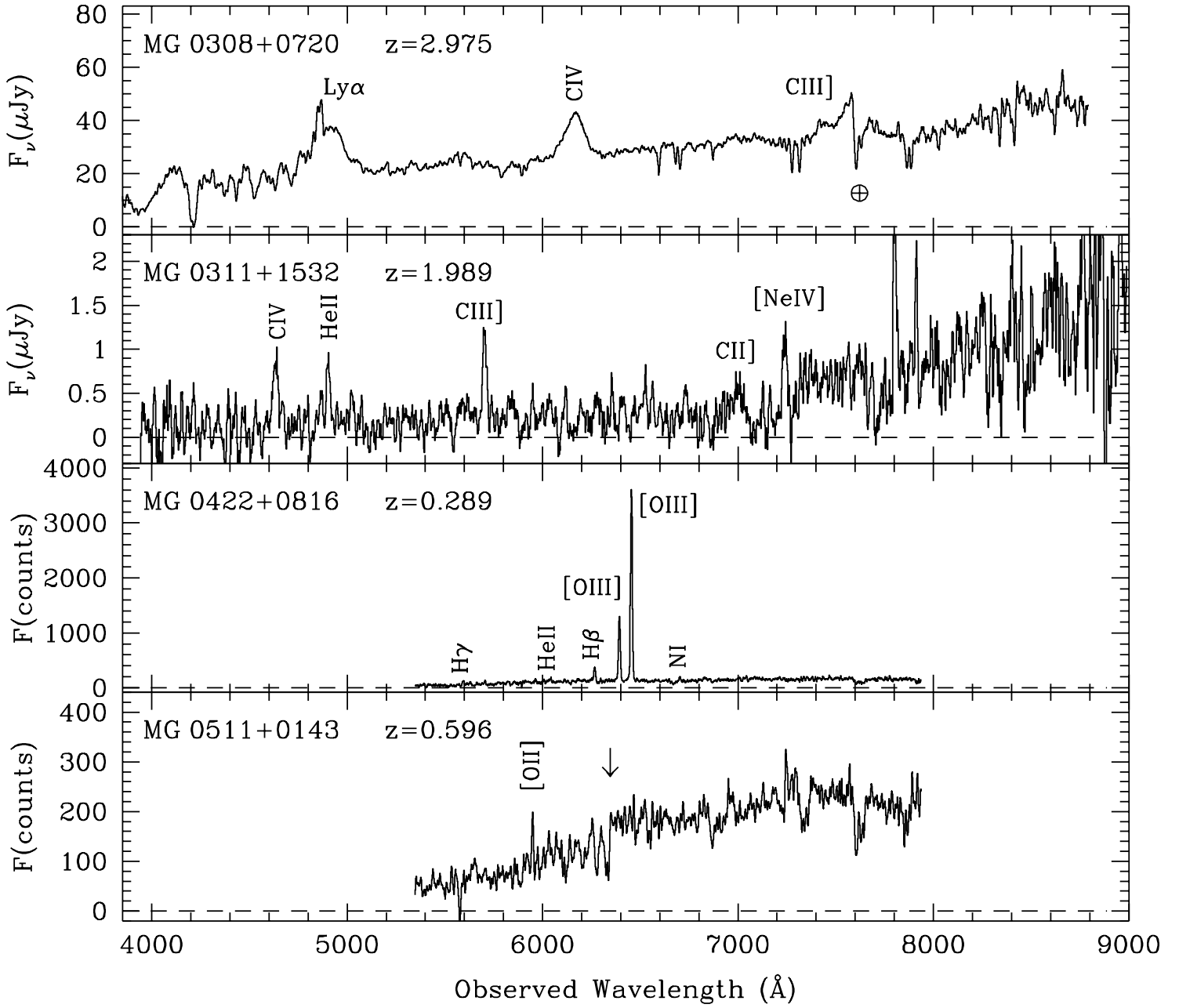
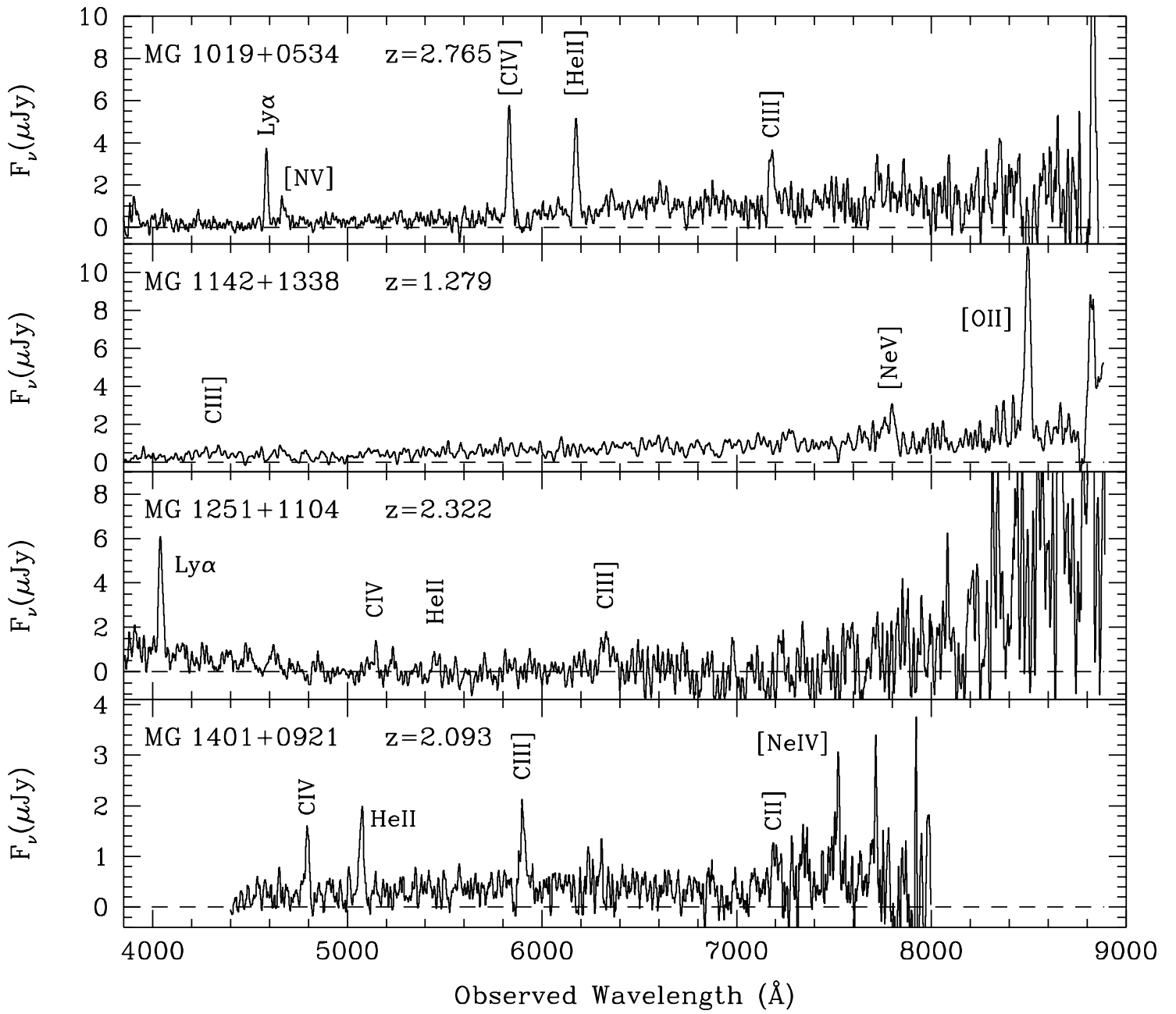
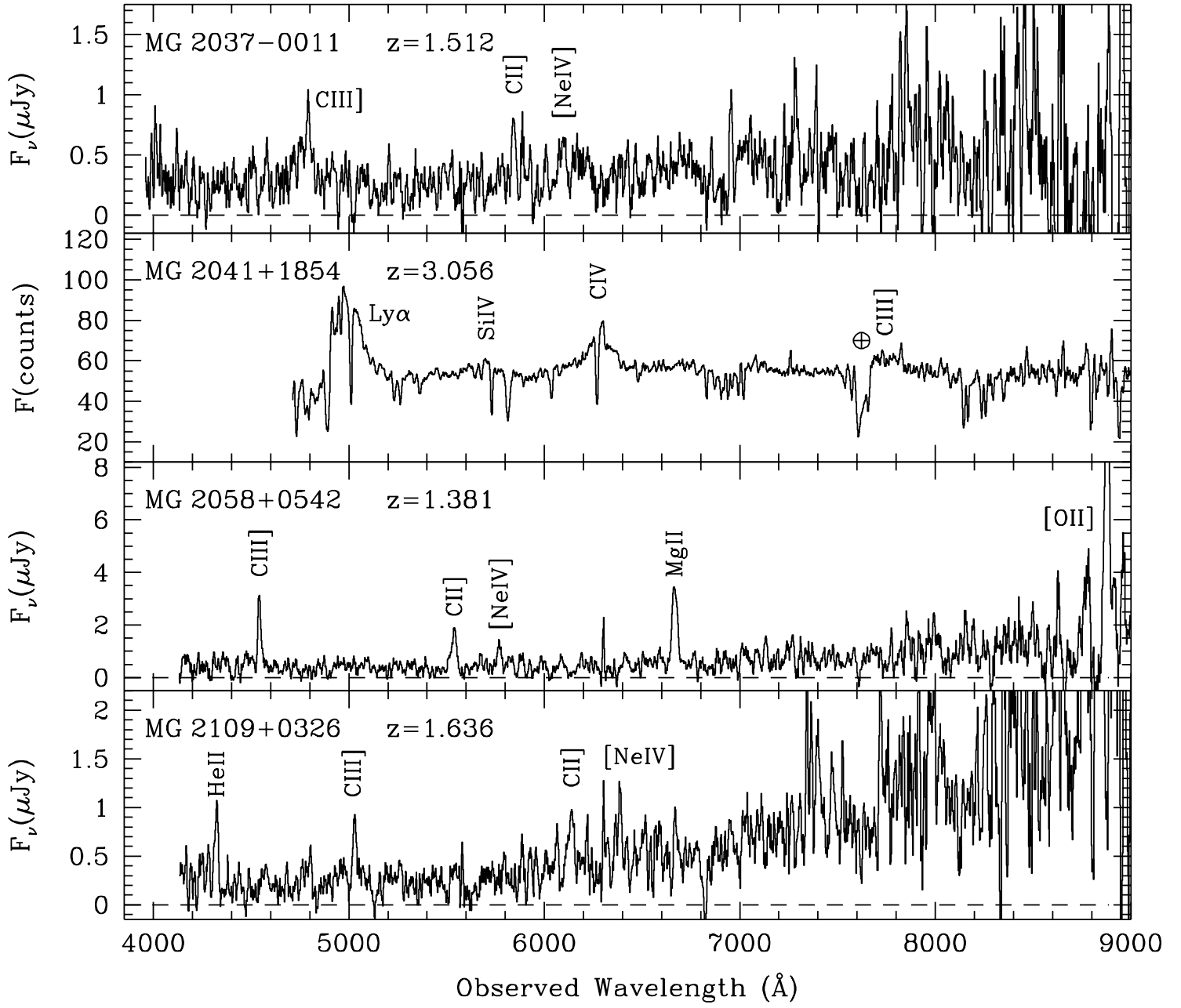
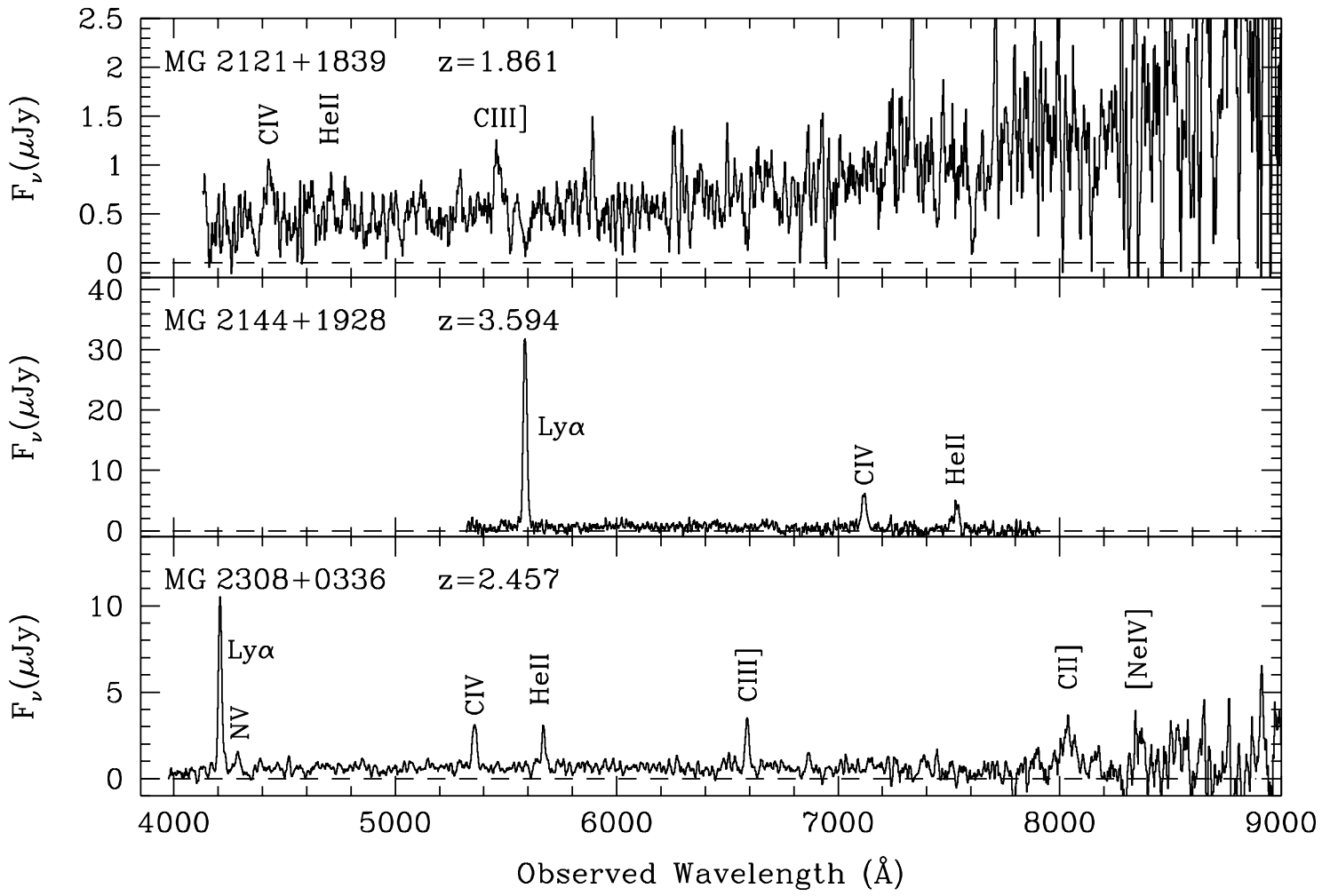


Fig. 2.— Spectra for the identifications, with prominent features indicated. Telluric absorption due to atmospheric water vapor (the “A-band”) is indicated by a cross within a circle. Vertical lines in the spectrum of MG 0148+1028 are explained in the text. The arrow labeled “D4000” in the spectrum of MG 0511+0143 refers to the 4000 Å break. Spectra of MG 1019+0534 and MG 2144+1928 are from Dey, Spinrad, & Dickinson (1995) and Maxfield et al. (1998) respectively.











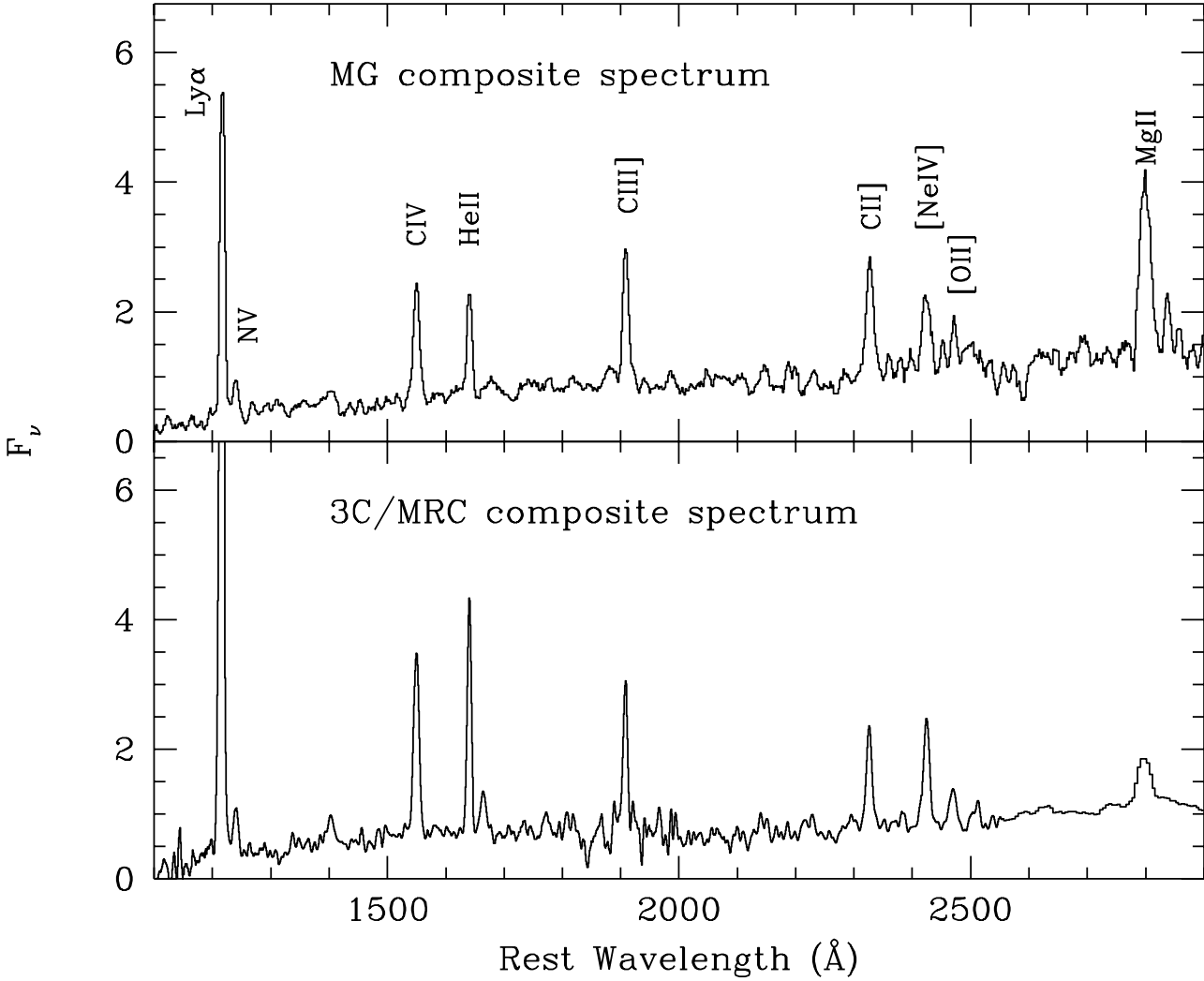


Fig. 3.— Composite MG (top) and 3C/MRC (bottom; McCarthy & Lawrence 1997) radio galaxy spectra, scaled with respect to the C III]  $\lambda 1909$  emission line. The 3C/MRC are typically higher radio flux density sources. Note the difference in relative strength of the carbon lines: whereas C IV  $\lambda\lambda 1549$  is the strongest of the carbon lines in the 3C/MRC composite, it is the weakest of the carbon lines in the MG composite spectrum, suggestive of a correlation between radio power and ionization state in distant radio galaxies.

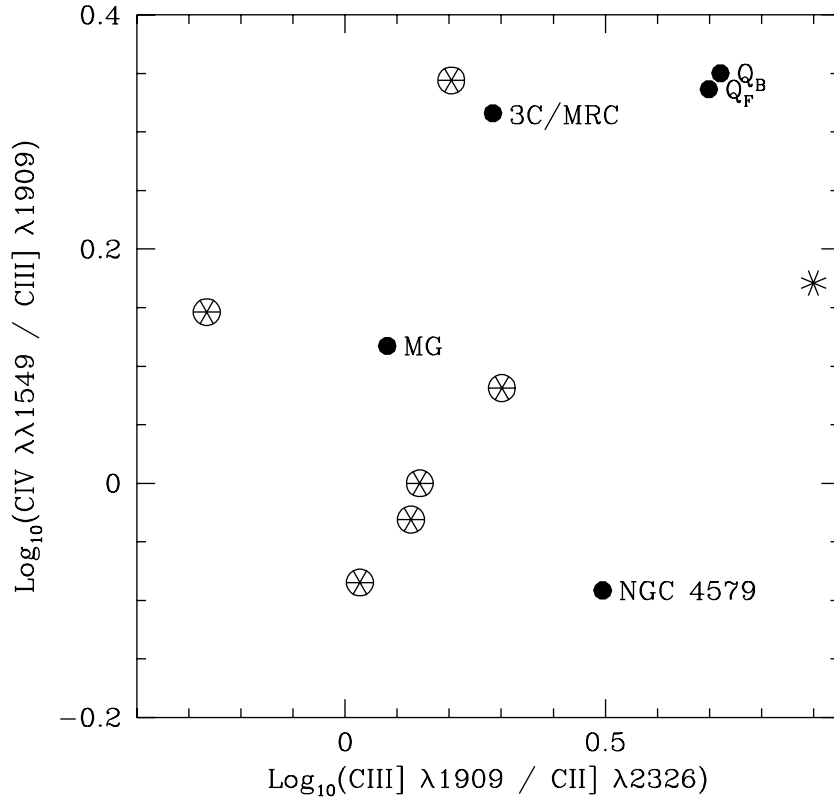


Fig. 4.— UV diagnostic diagram involving the various ionization stages of carbon. Pies represent individual MG galaxies. Filled-in circles with text refer to individual and composite spectra from Table 2:  $Q_B$  represents the quasar composite from Boyle (1990);  $Q_F$  represents the quasar composite from Francis et al. (1991); NGC 4579, a LINER galaxy, is from Barth et al. (1996). Note that the MG galaxies and composite MG exhibit lower ionization state carbon line ratios compared to the 3C/MRC composite and quasars. Asterisk represents CLOUDY model (see text).

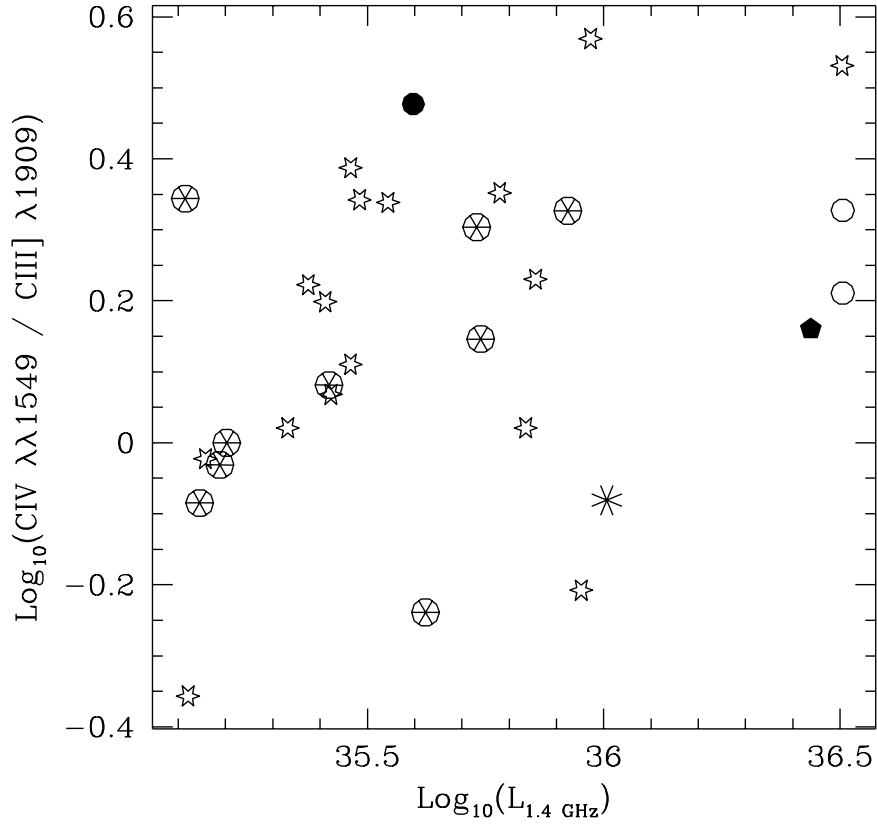


Fig. 5.— Ionization state-sensitive UV carbon line ratio plotted against rest-frame 1.4 GHz radio power for  $H_0 = 50 \text{ km s}^{-1} \text{ Mpc}^{-1}$  and  $q_0 = 0$ . Pies represent individual MG galaxies, open stars are from the ultra-steep sample (USS; Röttgering et al. 1994, van Ojik 1995), asterisk represents 3C 294 (McCarthy et al. 1990), filled pentagon represents 4C 41.17 (Dey et al. 1997), and filled/open circles represent 4C 00.54/4C 23.56 (Cimatti et al. 1998).

This figure "stern.fig1a.jpg" is available in "jpg" format from:

<http://arxiv.org/ps/astro-ph/9811344v1>

This figure "stern.fig1b.jpg" is available in "jpg" format from:

<http://arxiv.org/ps/astro-ph/9811344v1>

This figure "stern.fig1c.jpg" is available in "jpg" format from:

<http://arxiv.org/ps/astro-ph/9811344v1>